JOURNAL OF COLLOID AND INTERFACE SCIENCE **185,** 449–458 (1997)
ARTICLE NO. CS964536

Characterization of the Interface between a Rough Metal and Smooth Mica in Contact

J. M. LEVINS AND T. K. VANDERLICK[1]

Department of Chemical Engineering, University of Pennsylvania, 220 South 33rd Street, Philadelphia, Pennsylvania 19104-6393

Received May 10, 1996; accepted July 30, 1996

We introduce a technique to characterize, *in situ*, the solid–solid interface formed when a rough metal surface is placed in contact with a smooth mica surface. The technique is based on the use of extended spectral analysis of multiple beam interferometry in conjunction with the surface forces apparatus (SFA). The intensity versus wavelength spectra of light transmitted through the rough metal/mica interface is measured and compared to that transmitted through a smooth metal/mica interface. Interference theory is used to characterize the rough interface based on differences in the measured spectra. Roughness on the order of nanometers can be resolved. The key to our technique is the creation of a perfectly smooth metal/mica interface that is in all respects, except for roughness, identical to the metal/mica interface created in the SFA. We accomplish this by thermal evaporation of a metal film directly onto mica. We demonstrate the effectiveness of the technique by characterizing the structure of silver/mica and gold/mica interfaces. We also show how the technique can be used to investigate the exchange of fluids within the contact region.

Key Words: **roughness; multiple beam interferometry; surface forces apparatus.**

I. INTRODUCTION

An understanding of the nature of solid/solid interfaces is crucial to many areas of science and technology, including lubrication, wear, device manufacture, and the processing of powders and particulates. Solids interact with one another through the action of surface forces, which are governed by the chemistry and topography of the surfaces, as well as the nature of the medium trapped between them (1, 2). Of these factors, surface topography resulting from roughness is often the least controllable and the most difficult to characterize. Out of convenience, surface roughness is often neglected in theoretical studies of solid–solid interactions and avoided in associated experimental investigations.

Clearly roughness cannot be disregarded when two bodies are only slightly separated or in direct contact. As a general rule, roughness acts to reduce the strength of adhesion between two solids (3–5), but in ways that have made quantitative characterization formidable (4, 6). One of the key difficulties in this regard is that the structure of the interface can change as a function of loading or unloading, as a result of elastic and plastic deformations of surface asperities (7).

Although a variety of techniques are available for characterizing the topography of free solid surfaces—such as scanning–tunneling and atomic force microscopy (8–10)—none of these can be used if a surface is close to, or in contact with, another solid surface. One technique, however, that offers the potential to characterize the structure of a solid/solid interface is multiple beam interferometry (MBI) (11). This well-established technique is typically used to measure film thicknesses of either fluid or solid materials. This is basically accomplished by incorporating the film of unknown thickness into an interference filter; under ideal conditions, film thicknesses as small as angstroms can be resolved (12). When two rough solids are placed in contact, the medium trapped between them (air or liquid, for example) will vary in thickness from point to point, laterally across the nominal area of contact. Hence, MBI can be used to track these variations, thus providing a profile of the solid–solid interface.

The first person to take advantage of MBI to characterize angstrom-scale roughness was Bennett, who used the technique to measure the roughness of a variety of free surfaces (13). She employed MBI to track the thickness of the air layer trapped between a rough surface and a very smooth flat surface held micrometers above it. Since Bennett's work in the 1970s, no one has further developed or exploited this capability of MBI. Instead, MBI been put to most effective use in conjunction with the well-known surface forces apparatus (SFA) (1, 14, 15). This force-measuring device permits the separation between two curved surfaces to be changed in increments ranging from millimeters down to angstroms; MBI is used to measure the separation between the two opposed surfaces. In nearly all previous applications of the surface forces apparatus, molecularly smooth mica sheets have been employed. Hence lateral variations in the thickness of the medium trapped between the mica sheets

[1] To whom correspondence should be addressed.

0021-9797/97 $25.00

arise solely from the relative curvature of the opposing surfaces.

Recently we expanded the capabilities of MBI so that metallic surfaces could be used in the SFA (16). Our technique, called extended spectral analysis of multiple beam interferometry (ESA-MBI), relies on capturing the spectrum of light transmitted through the surfaces quantitatively, locally (over areas as small as possible), and in full detail (measuring intensity as a function of wavelength). Furthermore, the analysis of the captured spectra is based on predictions of classical interference theory, taking into account the optical properties of all materials which constitute the given interference filter. This is executed using the multilayer matrix method (17, 18).

We have previously described how ESA-MBI can be used to measure the separation between two smooth, flat surfaces, wherein one or both are metallic (16). In this paper we demonstrate how ESA-MBI can be used to characterize rough solid–solid interfaces, in particular those created when a rough metal is brought into contact with a smooth mica surface. As we shall show, the key to employing MBI for this purpose is the possibility of creating reference interferometers, which we call calibration filters, that are void of the rough interface, but are similar in all other respects.

This paper is divided as follows. Part II describes the general implementation of ESA-MBI for interferometers containing a rough metallic film. Part III describes the design and use of calibration filters in SFA experiments where a rough metal surface is placed in contact with a smooth mica surface. In Part IV, we use ESA-MBI to characterize the structure of gold/mica and silver/mica interfaces as created in the surface forces apparatus.

II. ACQUISITION AND ANALYSIS OF INTERFERENCE SPECTRA TRANSMITTED THROUGH A ROUGH SOLID/SOLID INTERFACE

Multiple beam interferometry requires the construction of an interference filter, which is composed of two reflective metal layers, separated by one or more layers of dielectric material. White light incident normal to the layers of the filter emerges as an intensity versus wavelength spectrum containing peaks. This spectrum is captured and measured. If the thickness of one or more layers in the filter is changed, it causes a change in the spectrum. Interference theory can be used to determine the change in film thickness from the measured change in the spectrum (16, 18).

Figure 1A shows a schematic of the filter we are using in the SFA. It consists of two thin mica sheets, cleaved so their surfaces are molecularly smooth, each coated on one side with a reflective metal film. The mica sheets are glued to cylindrical quartz supports (radius ca. 2 cm); one is glued with the bare mica exposed, the other with the metal film exposed. The cylinders are mounted in the SFA at right angles, with the mica surface opposed to the metal surface. The layers in this filter are thus metal–mica–medium–metal. Although the medium can be any dielectric fluid, we will assume it is air.

Due to the curvature of the cylindrical disks and the roughness of the metal films, the thicknesses of the layers in the filter are not uniform. As a result, the spectra transmitted through separate points of the filter are different. Note especially that the thickness of the air layer varies with both the curvature of the quartz supports and the roughness of the lower metal surface. When the metal and mica surfaces are placed in contact—as was done for all of the experiments that will be reported in this paper—the soft glue underneath the mica sheets deforms, creating a flattened region of metal/mica contact. This behavior, which will be described in more detail in Parts III and IV, conveniently creates a macroscopic contact region across which variations in the transmitted spectra can be attributed solely to variations in roughness. In the discussion which follows, however, we describe the general principles of the interferometric technique as applied to a filter with ''nonuniformities'' that could arise from both relative curvature and surface roughness.

Nonuniform filters can be characterized locally because ESA-MBI allows simultaneous measurement of spectra through many small contiguous sections of the filter. The size of the sections is governed by the hardware used to capture the transmitted spectra. The hardware consists of two pieces of equipment: a dispersion device and an intensity measuring device. A dispersion device acts to separate out light so that different wavelengths appear at different spatial positions. To do this, we use a scanning spectrometer (Thermo Jarrell Ash Corp., Model 82-000). The intensity measuring instrument that we use is a slow-scan charge-coupled device (CCD) camera (Photometrics Ltd., Series 200) that is mounted at the exit of the spectrometer (16). The image of the dispersed light is captured by a CCD chip, which is a rectangular grid of pixels; each pixel measures the intensity of light incident on it. Our CCD chip is composed of a 380×570 array of square pixels and is housed inside a liquid-cooled camera head, which allows very low intensities to be measured accurately.

Figures 1A and 1B are schematic pictures showing how the light transmitted through a filter is dispersed and then captured. A thin slice of light, shown superimposed on the filter in Fig. 1A, is admitted into the spectrometer through its entrance slit. The light is dispersed and then directed onto the CCD chip, which is aligned so the long axis is parallel to the dispersion direction of the spectrometer (Fig. 1B). Each row of the CCD chip measures the intensity versus wavelength profile of light transmitted through an individual section of the filter. One of the sections is drawn in Fig. 1A and its corresponding row of the CCD chip is shown in Fig. 1B by the dotted lines. The size of this section is set by the width of the entrance slit of the spectrometer, Δs, the height

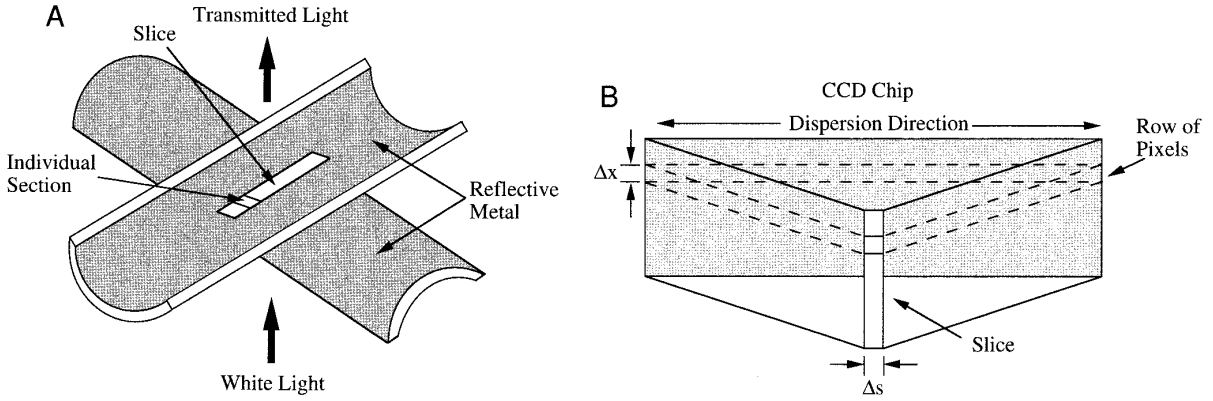

FIG. 1. (A) The crossed-cylinder filter in the SFA. (B) A schematic representation of the dispersion action of the spectrometer. A thin slice of light, shown superimposed on the filter in Figure 1A, is admitted into the spectrometer, and the light is dispersed. The dispersed light is then captured on the face of the CCD chip. A single row of the CCD chip is shown by the dotted lines, which measures the spectrum transmitted through an individual section of the filter, represented as a small square within the slice.

of the pixels, Δx, and the magnification of the emergent light en route to the spectrometer, M. The area of the section is simply $\Delta s \Delta x / M^2$.

There are two points that are important to understand about the measurement of transmitted spectra. First, each row of the CCD chip measures the average spectrum transmitted through a finite-sized section of the filter. The size of the section is determined as described above. For our experiments, $\Delta x = 23.2$ μm, $\Delta s = 100$ μm, and $M = 18.2$. Thus, each section is 1.3 by 5.5 μm. The second point is that the width of the pixels governs the detail that can be resolved in the wavelength direction (it has nothing to do with the size of the section). For our spectrometer the dispersion is 32.73 Å/mm, the pixel width is 23.2 μm, and thus each pixel spans across 0.759 Å wavelength. Since even the sharpest peaks in the spectra are typically 5 Å in width, we have very good resolution in the wavelength direction.

The size of the sections sets the scale of ''fine'' and ''gross'' nonuniformities within a filter. Fine variations are those which occur on a lateral scale that is much smaller than the dimensions of the sampled section. Gross variations occur over much greater lateral distances. For example, for the filter shown in Fig. 1A, the curvature of the mica sheets is a gross variation while the roughness of the metals may be either fine or gross.

Our method for characterizing nonuniformity within filters is based on two key phenomena that are readily predicted by interference theory (19). Specifically, variations in the thickness of the air layer cause, most predominantly, the peaks in the transmitted spectra to shift; thicker air layers shift the peaks to longer wavelengths. Variations in the thickness of the metal layers, however, do not significantly affect the locations of peaks in wavelength space, but mainly cause slight changes in the intensities of the peaks (decreasing the metal thickness increases the intensity).

Based on this insight, one of the most convenient ways to characterize nonuniformity within our filters is by tracking the locations of peaks in the spectra, which is equivalent to tracking variations in the thickness of the air layer. Each peak in the spectra is characterized by a single number, λ_p, which is an indicator of its location in wavelength space. For example, λ_p could be the wavelength of the center of a peak or the wavelength of the maximum intensity; some choices are more suitable than others, depending on the shapes of peaks transmitted through a filter. Clearly, this method does not take advantage of other information contained in the spectra. Since air thickness varies with both curvature of the mica and roughness of the lower metal surface, this method provides most of the critical information about nonuniformity without being too cumbersome.

The spectrum measured along each row of the CCD chip will generally contain several peaks. As described above, their locations will be different from row to row due to variations in the thickness of the air layer. Generally, the air thickness varies gradually enough that the peak locations along one row are not too far removed from those on the adjacent rows above and below. It is thus possible to generate several ''peak profiles,'' each of which is a plot of the location of a peak, λ_p, versus the row number of the CCD chip. Because the spectrum measured along each row is transmitted through a section of the filter, it is more informative to convert row number to ρ, where ρ is the position of the section of the filter along the slice.

The determination of λ_p is influenced by the fact that mica is a birefringent material (it has two indices of refraction) and thus every peak in the spectrum is actually the sum of two peaks slightly shifted from one another. For silver/mica filters, the peaks are sharp enough that birefringence results in clearly resolved doublets, and a peak profile can be generated for each. The locations of the peaks are determined by fitting them to Gaussian curves; λ_p is taken to be the best-fit mean (20). For most other metals, including gold, the

peaks are not sharp enough to be resolved into doublets—instead, birefringence causes a broadening of the peaks. In these cases, λ_p is found by locating the wavelength where half of the area under the broadened peak is to either side.

We mentioned in Part I that the concept of a peak profile was first introduced in 1976 by Bennett, who developed a ''FECO scanning interferometer'' to characterize the microscopic roughness of solid substrates (13). Bennett constructed her interference filter by coating a rough solid with silver and placing it opposite to another silver film supported on a smooth lens of fire-polished glass. The peak profile was used to map the surface of the rough solid. One drawback to her technique was that a video camera was used to capture the spectra, which required 2 hs of scanning to obtain a good signal-to-noise ratio. With a CCD camera, only about 5 to 10 s of exposure is necessary.

Although peak profiles provide much of the critical information, additional information can be gained by inspecting the transmissivity, T, versus wavelength profile of the spectrum. The transmissivity is simply the intensity of the transmitted light divided by the intensity of light incident to the filter (a description of how raw CCD measurements are converted to T is given in Ref. 16). Recently, we used interference theory to assess the impact of metal roughness on the spectrum transmitted through a finite-sized section of a filter (19), of the same type shown in Fig. 1A. We showed that the peaks in T become broader as the roughness of the metal increases. We also showed that roughness on the exterior surfaces of the filter had a negligible affect on the spectra, an observation that has been reported by others (21). Broadening can be understood by noting that the observed spectrum transmitted through a section of the filter is an average of all spectra transmitted through each point within the section. As a rule of thumb, the greater the standard deviation of the surface heights of the metal within that section, the greater the broadening of the peaks. We note here that our analysis (19) did not account for the scattering of light that is caused by roughness; however, we believe that the same general conclusions would hold under more rigorous analysis.

III. CREATION AND COMPARISON OF ROUGH AND SMOOTH SOLID/SOLID INTERFACES

Having described in the previous section the essential experimental and theoretical principles underlying the interferometric technique, we now turn to its practical application. Recall that our aim is to employ ESA-MBI to characterize the roughness of the interface between two surfaces—in this particular case, smooth mica and rough metal—that have been brought into contact using the SFA. As mentioned in Part II, when the surfaces are placed in contact, the soft glue underneath the mica sheets deforms to create a flattened region of metal/mica contact. Within this region, nonuniformities across the filter can be attributed to roughness, and not to curvature effects. The metal/mica interface within the contact region is characterized by measuring the spectra of light transmitted through the surfaces and comparing it against that transmitted through another, independent filter, where the metal/mica interface is smooth. Interference theory is used to interpret differences between the two spectra. Through the remainder of this paper, we will refer to the filter used in the SFA as the ''rough filter'' and the other as the ''calibration filter.''

A. Design of Rough Filters and Calibration Filters

Our metal films are prepared by condensing metal vapor, at very low pressure (approximately 10^{-7} Torr), onto the molecularly smooth mica sheets, a technique commonly referred to as thermal evaporation. (This procedure for preparing metal-coated mica sheets is described in detail in the Appendix.) Because the mica sheets are molecularly smooth, the interface between the mica and condensed metal is also smooth. However, the exposed surface of the metal film, at the vacuum/metal interface, is microscopically rough (22–24).

A rough filter is constructed by using the SFA to place a smooth mica surface into contact with a rough metal surface (Fig. 1A). Generally, when two curved elastic bodies are brought close together, they will deform about the region of closest approach (25–29). For the crossed cylinder filters used in the SFA, the soft glue holding the mica sheets to their supports undergoes the greatest deformation (29). When the rough filter is constructed, a flattened region of metal/mica contact forms, typically several tens of micrometers in diameter. This deformation is clearly apparent in the peak profiles and it is used to identify the region of metal/mica contact.

A calibration filter is constructed by coating a mica sheet, of thickness identical to that of the upper mica sheet in Fig. 1A, on both sides with metal. Such a double-coated mica sheet has two smooth metal/mica interfaces. Provided the metal films of the calibration filter are the same thickness as those in the rough filter, the only difference between the two filters is that one of the metal/mica interfaces in the rough filter is rough.

Although it is not necessary to place the calibration filter inside the SFA, we did so when measuring the spectra transmitted through it. This was done to ensure that the optical setup surrounding the calibration filter—which consists of several quartz lenses, two prisms, and a 10-fold magnifying lens through which the light passes en route to the spectrometer—was the same as that surrounding the rough filter. This procedure eliminated concerns that dissimilarities between the spectra measured for both filters were due to differences in the optical setup and not roughness. Finally, we point out here that even though the calibration filer is supported on a cylindrical lens—and hence the filter is curved—the peak

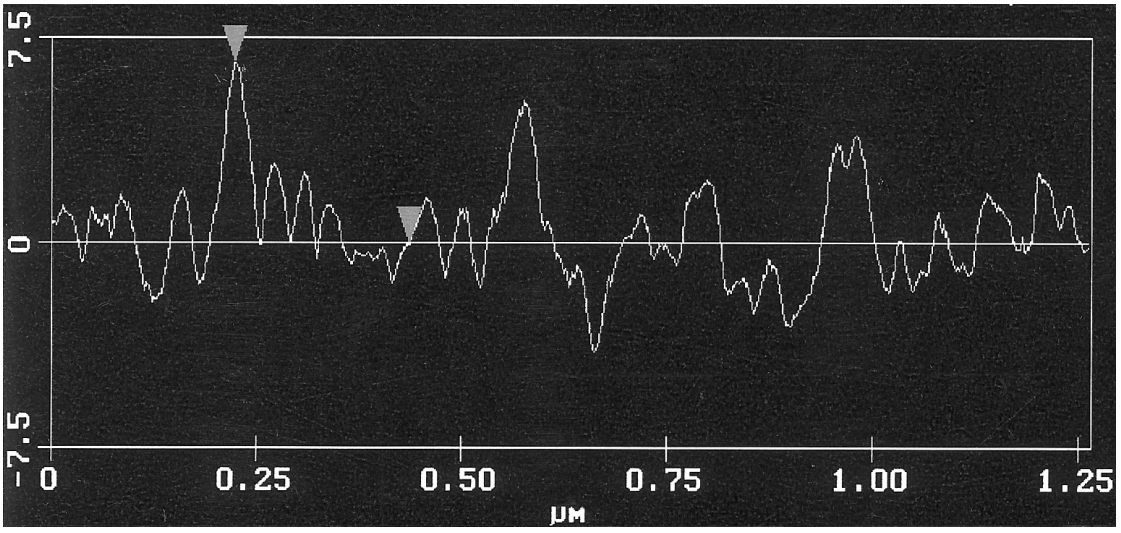

FIG. 2. AFM scan across a 300 Å thick silver film on mica. The vertical scale is in nanometers; the two inverted triangles shown in the surface profile are 66 Å apart.

profiles are flat because the interferometer layer thicknesses are uniform.

B. Interpretation of ESA-MBI Measurements

The essence of interpreting ESA-MBI measurements is based on comparing the spectra transmitted through a rough filter with that transmitted through a calibration filter. With regard to the latter, the peak profiles for a calibration filter should be flat; i.e., λ_p should be constant for all ρ. Any variations in λ_p can be attributed to noise in the measurement of transmitted spectra.

Roughness at a metal/mica interface will cause the peak profile for a rough filter to be shifted to a longer wavelength than the peak profile for its companion calibration filter. The metal/mica contact region can be identified by finding the part of the rough filter's peak profile that is flattened. If the metal/mica surface is rough on a gross scale, the values of λ_p will vary across the flattened region, reflecting the gross roughness. Bona fide gross features (manifested as differences in spectra from one section to another) should be mirrored in all of the captured peak profiles, a useful fact that is valuable when trying to distinguish such variations from noise.

For a given filter, the rougher the interface the larger the degree of shift away from the calibration filter (19). Basically, the shift is induced because of trapped dielectric material, typically air, between the mica and the metal. The exact amount of the degree of the shift will depend on the topography of the metal surface, as well as on the optical properties and thicknesses of the layers within the filter (16).

Further information regarding the topography of the metal/mica interface can be gained by comparing the shapes of the peaks in T for the rough filter against those for the calibration filter. As explained in the previous section, the rough filter's peaks should be broader. By invoking a model of the metal topography, T can be predicted using interference theory. Although it is possible to rule out topographies that do not match the measured spectra, it is not possible to do the inverse, i.e., to determine exactly the topography of the metal surface. However, it is reasonable to assume that topographies that are consistent with the measured T will have similar characteristic length scales, or roughness. It is thus possible to use ESA-MBI to determine this characteristic length scale. One picks a reasonable topography that generates peaks of the correct shape and then varies the roughness until the locations of the predicted peaks match those measured. The inputs required to predict the spectra are the thicknesses and refractive indices of all the layers within the filter (16, 18).

On a final note, it is not necessary to invoke a model to characterize *changes* in roughness within a filter. A general phenomenon, which can be verified from calculations, is that for a given model of topography, the shifting of the peaks to longer wavelengths varies linearly with the characteristic length of roughness.

IV. RESULTS: CHARACTERIZATION OF SILVER/MICA AND GOLD/MICA INTERFACES

The techniques and concepts described in Parts II and III were used to characterize the interface formed when mica is brought into contact with two different metals: silver and gold. As a point of reference, we first describe the ''free'' roughness of these metal surfaces as they exist in laboratory air, as measured using an atomic force microscope (AFM). The AFM scans showed the films to be polycrystalline; the

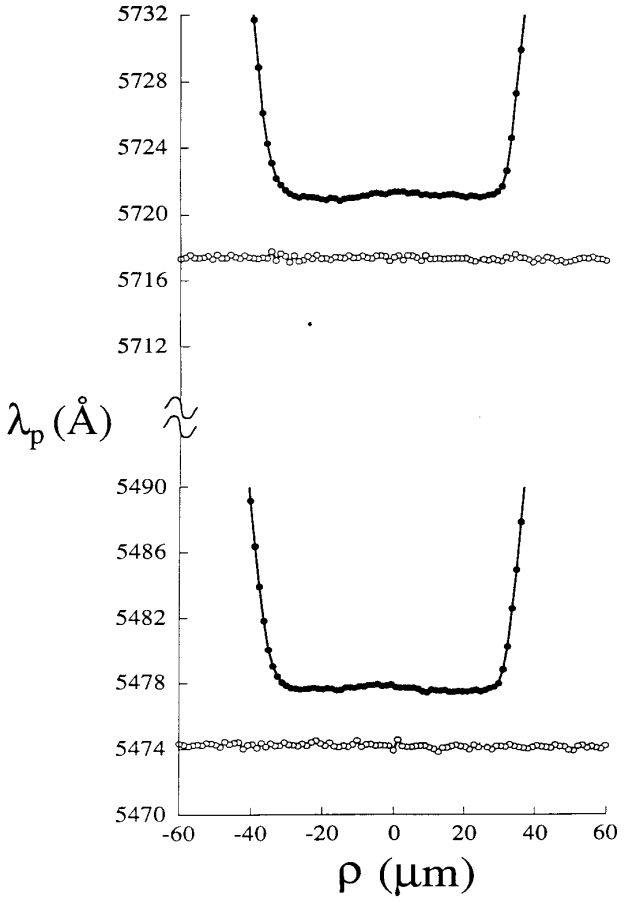

FIG. 3. Peak profiles measured for silver/mica filters. The rough filter (solid circles), was constructed by placing bare mica in contact with a silver film. The calibration filter (open circles) was constructed by doubly coating a mica sheet. Both filters were coated on one side with 400 Å of silver and on the other with 500 Å. For the rough filter, the bare mica surface was brought into contact with the 500 Å thick film.

silver grains are approximately 25 nm in diameter and the gold grains approximately 10 nm in diameter. The silver surface was dominated by a few tall grains which stood up like ''spikes'' about 10 per square micrometer, approximately 5–8 nm taller than the rest of the silver surface; a typical surface profile is shown in Fig. 2. The heights of the gold grains appeared more normally distributed, with an average roughness of about 2 nm. Although we performed AFM scans on only one film of each metal type, all films used in this study were prepared under similar conditions.

Shown in each of Figs. 3 and 4 are peak profiles for a calibration filter and its companion rough filter. Silver films were used in the filters for Fig. 3 and gold films for those in Fig. 4. Two graphs are drawn in each figure, representing two adjacent peak profiles that were distilled from the measured spectra. As described in Part II, each data point on the graphs represents the wavelength, λ_p, of a peak in the measured spectrum transmitted through a 1.3 by 5.5-μm section of the filter. The abscissa, ρ, is the location of the section along the slice of light admitted into the spectrometer. For convenience, we have arbitrarily defined ρ to be zero at the middle of the flattened region of the peak profile.

As expected, the peak profiles for the calibration filters are fairly flat. As described in Part III, the noise in λ_p sets the limit to which we can detect gross variations in the rough filters. It is apparent from Figs. 3 and 4 that the noise is significantly less than 1 Å. Close inspection of both figures shows that the peak profile for the gold calibration filter is noisier than that for the silver filter. Most likely, this is because the peaks in the spectra of silver-coated filters are much sharper than those for gold-coated filters. As a point of reference, the standard deviation in λ_p is 0.11 Å for the silver filter and 0.24 Å for the gold filter.

The most important observation that can be made about the rough filters is that their peak profiles, along the flattened metal/mica contact region, are shifted to longer wavelengths than the peak profiles for the calibration filters. It is also clear in Figs. 3 and 4 that the peak profile along the contact region of the rough filters is fairly flat, nearly as flat as that

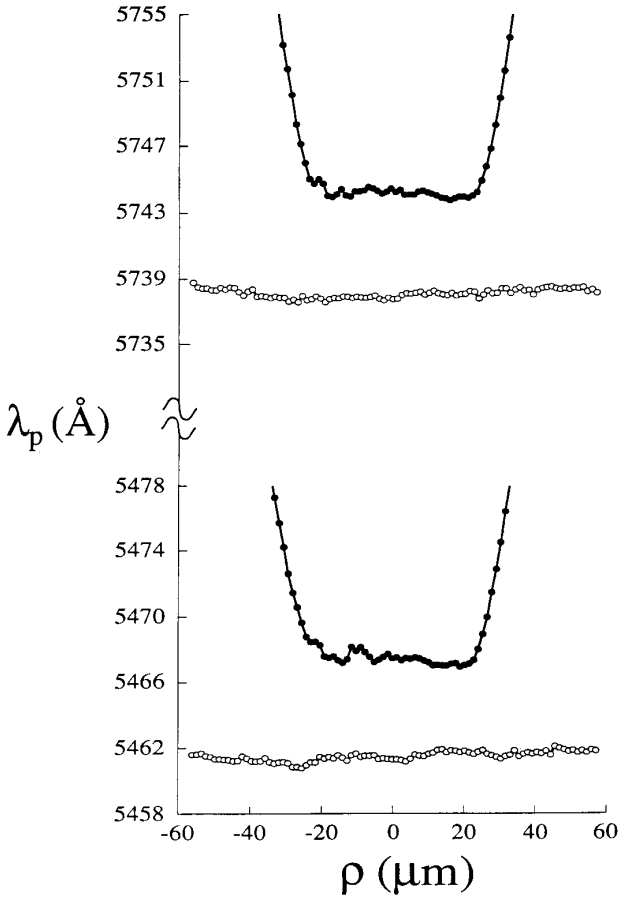

FIG. 4. Peak profiles measured for gold/mica filters. The rough filter (solid circles), was constructed by placing bare mica in contact with a gold film. The calibration filter (open circles) was constructed by doubly coating a mica sheet. Both filters were coated on both sides with 525 Å of gold.

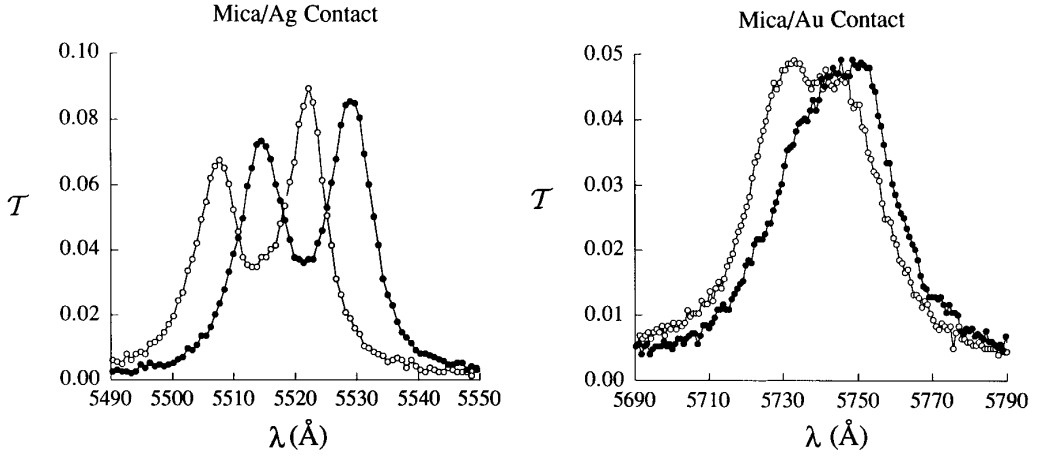

FIG. 5. Transmissivity, T, versus wavelength spectra measured through a single section of silver/mica and gold/mica filters. Only a part of the measured spectra is shown in each plot. The solid circles are for the rough filters and the open circles are for the calibration filters. Note that the gold/mica filters are the same ones whose peak profiles are shown in Fig. 4.

for the calibration filters. It thus seems that the metal/mica interfaces are not rough on a gross scale. The rough filter in Fig. 3, however, may have a small hump in the middle of the contact region. The hump is tiny, but it is present in both peak profiles, indicating that it may be a real feature. For the plots in Fig. 4, the only feature that appears in both peak profiles is a small kink on the left-most edge of the contact region.

To probe further the topography of the interfaces, we examine the shapes of peaks in the spectra transmitted through silver/mica and gold/mica rough filters. Figure 5 shows a typical plot of T for both. The spectrum measured along a single row of the CCD chip is shown (i.e., a single value of ρ). The most important observation that can be made about Fig. 5 is that the shapes of the peaks in the spectrum for calibration filters and rough filters are nearly the same. (This observation holds for all spectra measured at different ρ.) As we stated in Part II, one of our previous findings was that roughness at a metal/mica interface causes a broadening of the peaks. Thus, the simplest model that would support the spectra in Fig. 5 is one where the metal surfaces are mostly smooth, except for a few thin spikes sticking upward.

Using this ''spike model,'' we can determine the characteristic lengths of the roughness of our silver and gold films. This is equal to the height of the spikes, or equivalently the thickness of the air gap, assuming air occupies the space between the bulk metal and the mica. Interference theory is used to calculate the thickness of the air gap so the predicted peaks best match those measured. We have performed these calculations for the filters shown in Figs. 3 and 4. The thickness of the air gap for each value of ρ along the flattened metal/mica contact region was calculated, and these values were averaged to yield an overall roughness. This was done for both of the peak profiles measured for each filter. For the silver/mica interface in Fig. 3, the calculated air gap is 30 ± 2 Å for both peak profiles. For the gold/mica interface in Fig. 4, the air gap is 47 ± 4 and 44 ± 4 Å for the upper and lower profiles, respectively. The uncertainty reported reflects the scatter arising from the fact that the region of contact is not perfectly flat.

In performing the calculations just described, we used the refractive indices of mica and metal described in a previous publication (16). Our metal thicknesses are measured during preparation (see the Appendix). The mica thickness is determined by finding the best match of the measured spectra transmitted through the calibration filter against that predicted.

Our determined air gap of 30 Å for the silver/mica interface is thinner than the height of the silver spikes measured with the AFM. In light of our other observations that the roughness of silver and gold films decreases over time in contact with mica (30, 31), this is not surprising. It is probable that compression of the spikes occurs upon silver/mica contact. For gold/mica contact, the determined air gap of 46 Å is approximately 25 Å thicker than the average roughness of the gold surface measured with the AFM. It is possible that this discrepancy is due to a few tall grains on the gold surface that were not observed during the AFM scan.

Clearly, even in the presence of adhesive forces, the intimacy of contact between the two materials is not perfect: significant dielectric material exists between the metal and mica surfaces. The presence of a rough gap at the metal/mica interface sets the stage for a unique type of experiment, wherein the air trapped between the surfaces is exchanged for another dielectric fluid, specifically a liquid formed by capillary condensation. ESA-MBI can be employed to monitor the exchange of fluids, thus creating the opportunity to study, for example, the penetration of nanometer-scale pores by a condensing liquid. The results of preliminary capillary

condensation experiments are described below. The results are particularly suited to this paper because, as we shall show, they can be used to check our roughness measurements.

A droplet of cyclohexane was condensed about the same gold and mica surfaces in Fig. 4. First, peak profiles for gold/mica contact in air were measured, as discussed above, and then a tissue soaked with cyclohexane was placed in the bottom of the SFA. The SFA was sealed and, after a few minutes, the air became saturated with cyclohexane vapor. Cyclohexane condensed around the contact region, forming a droplet held between the mica and metal surfaces. The droplet rapidly grew outward from its center, i.e., the middle of the metal/mica contact region. A meniscus readily formed about the region of contact; its presence is apparent from a kink observed in the tails of the peak profiles that is caused by the sudden change in refractive index at the droplet's edge. The droplet continued to grow for a few minutes, until its diameter was on the order of a few millimeters, much greater than the diameter of the metal/mica contact region.

Figure 6 shows the peak profiles measured before and right after the droplet formed. As is readily seen, the peak profiles shifted to longer wavelengths, a result of cyclohexane penetration within gold/mica interface (a quantitative analysis of this effect is discussed below). Figure 6 also shows that the area of deformed gold/mica contact increased dramatically. It appears that the surface tension of the cyclohexane exerted some force on the surfaces, squeezing them together. Over longer times, however, as the size of the condensed liquid drop grew well beyond the region the contact, the area of deformed contact began to decrease back to the area as measured in air (although the shift in peak profiles remained the same).

The shift in peak profiles to longer wavelengths is a direct manifestation of the increase in refractive index associated with the exchange of fluid (from air to liquid cyclohexane) trapped between the mica and the metal. We take advantage of this phenomenon to perform a check on the roughness of the confined metal as quantified using the methods and procedure described in this paper. For both peak profiles in Fig. 6, the measured shift of the flattened portions was 0.7 $\pm$ 0.1 Å. This number was determined by averaging λ_p for each value of ρ along the flat parts of the peak profiles. The uncertainty is due to the fact that the profiles are not perfectly flat. Using a spike model for the roughness with associated gap thicknesses as previously determined (47 $\pm$ 4 and 44 $\pm$ 4 Å for the upper and lower profiles, respectively), we use interference theory to predicted the shift in λ_p caused by changing the medium from that of air (refractive index of 1.000) to that of cyclohexane (refractive index 1.427). We find this to be 0.7 and 0.8 Å for the upper and lower profiles, respectively. These predictions are in excellent agreement with those measured.

One final point we wish to make is that, although a model of surface topography must be invoked to determine quantitative roughness values from ESA-MBI measurements, changes in the roughness of a particular filter can be quantitatively determined without a model. We have found that silver films can be roughened by simply heating them, in air, to approximately 160°C for a few minutes. Figure 7 shows two peak profiles measured for the same set of silver and mica surfaces. The first peak profile was taken for silver/mica contact (see Fig. 3). The second was measured after separating the surfaces, heating the silver film, and placing the surfaces back into contact. The peak profile for the heat-treated silver/mica interface is shifted to longer wavelengths. Because the shift away from the calibration filter is twice as great for the heated silver as for the unheated silver, it can be concluded that the heated silver is about twice as rough. Note that the peak profile for the calibration filter did not change with heating.

We used an AFM to image a heated silver surface. The grains on the heated surface were about 1000 Å in diameter and the few tall spikes were typically 100 to 120 Å above the rest of the silver surface, instead of 50 to 75 Å for the unheated surface. This is in reasonable agreement with our observation that the silver becomes twice as rough upon heating.

On a final note, it is clear in Fig. 7 that the size of the metal/mica contact region is smaller for the heated silver than for the unheated silver. This is only one example of how roughness at the interface between two solids in contact dramatically affects their deformation and adhesion. We have used ESA-MBI to study this in detail, and it is the subject of another publication (31).

CONCLUSIONS

Our technique employs extended spectral analysis of multiple beam interferometry to characterize the interface between a microscopically rough metal film and smooth mica. The two surfaces are placed in contact with the surface forces apparatus. A key to this technique is the creation of a ''calibration'' metal/mica interface that is identical to the one created in the SFA with the sole exception that it is perfectly smooth.

Using our technique, we were able to ''peer'' at the solid–solid interface, locally and throughout the region of nominal contact. We found that, even in the presence of adhesive forces strong enough to noticeably deform the surfaces, contact between the metal and the mica is far from being perfectly intimate. Instead, the equivalent of a dielectric filled gap exists between the surfaces. The thickness of this gap can be accurately measured and we found it to be approximately as thick as the height of the tallest asperities of the metal, as measured using an atomic force microscope. Furthermore, we used the technique to observe the condensation of liquid within the gap, an experiment which suggests excit-

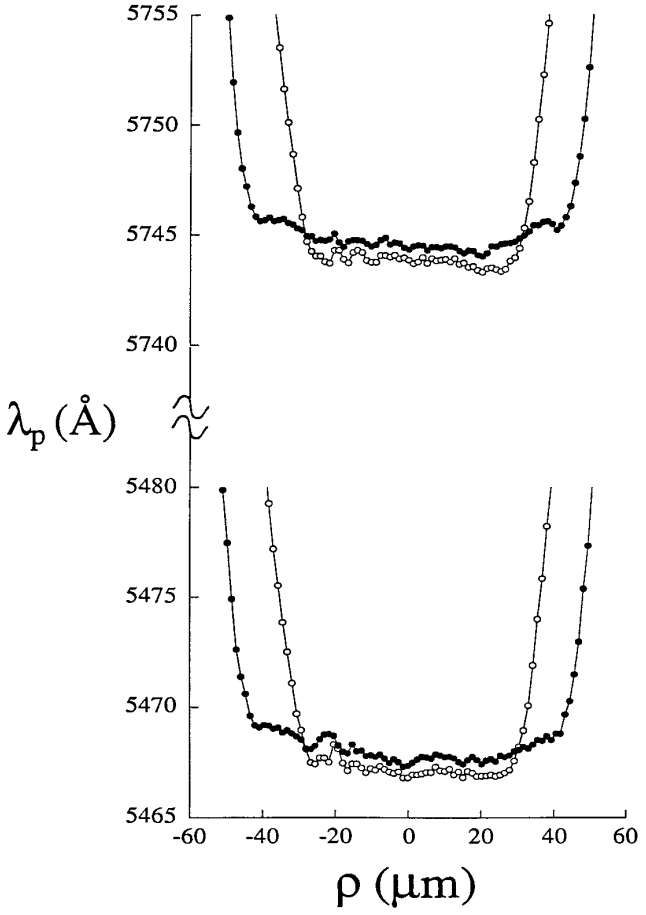

FIG. 6. Peak profiles for gold/mica contact in air (open circles) and 10 min after saturating the interior of the SFA with cyclohexane vapor (filled circles).

ing opportunities to investigate capillary condensation of liquids within microscopic gaps or pores.

The SFA, which for several decades has been used to measure forces acting between opposed solid surfaces, has been restricted almost exclusively to materials with molecularly smooth surfaces. The combination of our technique with the SFA provides one of the most powerful tools for characterizing rough solid/solid interfaces *in situ.* Thus, it is possible to carry out new experiments to study the influence of surface topography on the forces acting between solid surfaces, either in contact or separated by a fluid medium. Such studies promise to have a significant impact on our understanding of many phenomena, including adhesion (31) and lubrication.

APPENDIX: CONSTRUCTION OF ROUGH FILTERS AND CALIBRATION FILTERS

Muscovite mica is cleaved into a thin sheet, approximately 3–4 μm thick, of uniform thickness. At least two squares of mica (1 cm on a side) are then cut from this sheet and placed on a large thick support sheet of freshly cleaved mica. Metal films (gold or silver) are coated onto the support sheet, thus covering the exposed faces of the small squares, by thermal evaporation from a tungsten boat in a turbo-pumped Pyrex bell-jar system. The evaporation rate and the final film thickness are measured using a quartz crystal monitor. We used metals of 99.999% purity. Base pressure during all our evaporations was better than 8×10^{-7} Torr. Rates of evaporation were 2.8 Å/s for gold and between 3.5 and 4.0 Å/s for silver.

Two of the square mica sheets are then removed from the support sheet and glued to cylindrical quartz disks using the epoxy resin Epon 1004, with the metal side against the resin and the bare mica surface up. One of the quartz disks is placed in the SFA, its bare mica surface becoming part of the rough filter. The other quartz disk is placed back in the evaporator to be coated again with a metal film, thus creating the calibration filter. Along with the calibration filter, a new sheet of thin mica uncoated on either side, that had been glued to a quartz disk, is also coated with metal. The new sheet serves as a substrate for the second metal film to be used in the rough filter.

We finally note that interference theory can predict transmitted spectra so accurately that the calibration filter does not have to be constructed. Instead, its spectrum can be predicted. Typically, the only unknown necessary to predict the spectrum is the mica thickness. A method of determining mica thickness is to construct a mica/mica filter in the following way: Two mica sheets, each of the same thickness as the one used in the rough filter and each coated with a reflective film on its backsides, are placed in contact so the bare mica surfaces are touching. The thickness of the mica sheets can be determined by matching the measured spectra transmitted through the mica/mica contact region against theory (12, 16). Note that this method is advantageous only

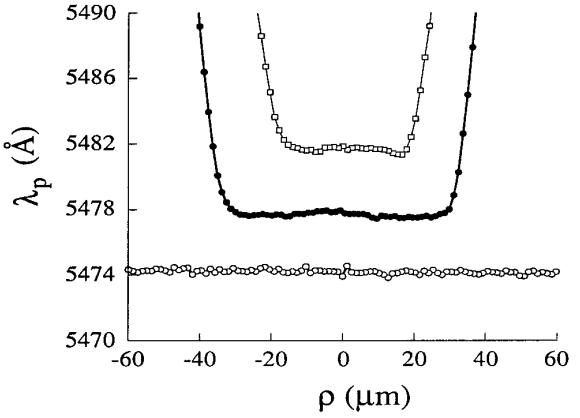

FIG. 7. Peak profiles for silver/mica filters before heating the silver surface (solid circles) and after heating the silver in air to 160°C for three minutes (open squares). The peak profile for the calibration filter is also shown (open circles). The filter is the same one as in Fig. 3.

if it is more convenient to prepare a mica/mica filter than a calibration filter.

ACKNOWLEDGMENTS

We gratefully acknowledge the support for this work provided by the David and Lucile Packard Foundation, the National Science Foundation Presidential Young Investigator Program (Grant CTS-89-57051), the National Science Foundation MRL Program (Grant DMR91-20668), and a Henkel Corporation Colloid and Surface Science Fellowship awarded to J.M.L. We also thank Jack Josefowicz for obtaining the AFM images of our metal films.

REFERENCES

1. Israelachvili, J. N., *Intermolecular and Surface Forces.* Academic Press, London, 1985.
2. Ennis, B. J., Green, J., and Davies, R., *Chem. Eng. Prog.* **32,** (April 1994).
3. Kendall, K., *Science* **263,** 1720 (1994).
4. Tabor, D., *J. Colloid Interface Sci.* **58,** 2 (1977).
5. Johnson, K. L., *Contact Mechanics.* Cambridge Univ. Press, New York, 1985.
6. Fuller, K. N. G., and Tabor, D., *Proc. R. Soc. Lond. A* **345,** 327 (1975).
7. Thomas, R. C., Houston, J. E., Michalske, T. A., and Crooks, R. M., *Science* **259,** 1883 (1993).
8. Binning, G., Rohrer, H., Gerber, C., and Weibel, E., *Phys. Rev. Lett.* **50,** 120 (1983).
9. Binnig, G., Quate, C. F., and Gerber, C., *Phys. Rev. Lett.* **56,** 930 (1986).
10. Wickramasinghe, H. K., *J. Vac. Sci. Technol. A* **8,** 363 (1990).
11. Tolansky, S., *Multiple-Beam Interferometry of Surfaces and Films.* Oxford Univ. Press, London, 1948.
12. Israelachvili, J. N., *J. Colloid Interface Sci.* **44,** 259 (1973).
13. Bennett, J. M., *Appl. Optics* **15,** 2705 (1976).
14. Tabor, D., and Winterton, R. H. S., *Proc. Roy. Soc. A.* **312,** 435 (1969).
15. Israelachvili, J. N., and Adams, G. E., *J. Chem. Soc. Farad. Trans. I* **74,** 975 (1978).
16. Levins, J. M., and Vanderlick, T. K., *Langmuir* **10,** 2389 (1994).
17. Born, M., and Wolf, E., *Principles of Optics.* Pergamon, New York, 1980.
18. Clarkson, M. T., *J. Phys. D* **22,** 475 (1989).
19. Levins, J. M., and Vanderlick, T. K., *J. Colloid Interface Sci.* **158,** 223 (1993).
20. Quon, R. A., Levins, J. M., and Vanderlick, T. K., *J. Colloid Interface Sci.* **171,** 474 (1995).
21. Eastman, J. M., *in* ''Physics of Thin Films,'' (G. Haas and M. H. Francombe, Eds.) Vol. 10, pp. 167–226. Academic Press, New York, 1978.
22. Buchholz, S., Fuchs, H., and Rabe, J. P., *J. Vac. Sci. Technol. B.* **9,** 857 (1991).
23. Chidsey, C. E. D., Loiacono, D. N., Sleator, T., and Nakahara, S., *Surf. Sci.* **200,** 45 (1988).
24. Golan, Y., Margulis, L., and Rubinstein, I., *Surf. Sci.* **264,** 312 (1992).
25. Parker, J. L., and Attard, P., *J. Phys. Chem.* **96,** 10,398 (1992).
26. Attard, P., and Parker, J. L., *Phys. Rev. A* **46,** 7959 (1992).
27. Johnson, K. L., Kendall, K., and Roberts, A. D., *Proc. R. Soc. London A* **324,** 301 (1971).
28. Derjaguin, B. V., Muller, V. M., and Toporov, Y. P., *J. Colloid Interface Sci.* **53,** 314 (1975).
29. Horn, R. G., Israelachvili, J. N., and Pribac, F., *J. Colloid Interface Sci.* **115,** 480 (1987).
30. Levins, J. M., and Vanderlick, T. K., *J. Phys. Chem.* **96,** 10,405 (1992).
31. Levins, J. M., and Vanderlick, T. K., *J. Phys. Chem.* **99,** 5067 (1995).